Anchoring an Iridium Pincer Complex in a Hydrophobic Microporous Polymer for Application in Continuous-Flow Alkane Dehydrogenation

Michaela König[+],[a] Michael Traxler[+],[a] Maik Alexander Rudolph,[b] Johannes Schmidt,[a] Hüseyin Küçükkeçeci,[a] Reinhard Schomäcker,[b] and Arne Thomas*[a]

An iridium pincer complex {p-KO-C$_6$H$_2$-2,6-[OP(t-Bu)$_2$]$_2$}Ir(C$_2$H$_4$) is immobilized in a propyl bromide-functionalized microporous polymer network using the concepts of surface organometallic chemistry. The support material enables the formation of isolated active metal sites embedded in a chemically robust and highly hydrophobic environment. The catalyst maintained high porosity and – without prior activation – exhibited high activity in the continuous-flow dehydrogenation of cyclohexane at elevated temperatures. The catalyst shows a stable performance for at least 7 days, even when additional H$_2$O was co-fed, owing to its hydrophobic nature.

Introduction

Alkanes can be extracted from various sources, including natural gas, mineral oil, coal, and biomass. Some of these alkanes (C9–C19) are utilized as fuels, but abundant leftover alkanes have poor application. In comparison, low molecular-weight alkenes and aromatic compounds are essential key intermediates in the synthesis of a multitude of fine chemicals or polymers on an industrial scale. Therefore, the conversion of alkanes to high-value alkenes or arenes is of great commercial interest.[1] Dehydrogenation reactions are realized industrially on a large scale at high temperatures (400–600 °C) utilizing solid metal catalysts, however with low product selectivities as well as little energy efficacy.[2] Since their discovery, molecular catalysts featuring tridentate pincer ligands are widely explored and are applied for versatile reactions, such as hydrogenation, coupling, hydrogen transfer, aldol and Michael reactions as well as dehydrogenation or even tandem reactions involving alkane dehydrogenation.[3–12] In the field of alkane dehydrogenation iridium pincer complexes have received great interest due to their high activity as well as regioselectivity for the formation of terminal olefins, enabled by the relatively mild reaction temperature of around 240 °C compared to currently applied industrial processes.[13]

Combining homogeneous and heterogeneous catalysis by immobilizing a molecular catalyst onto suitable supports has been investigated widely in recent years. Thereby, the advantages of homogeneous as well as heterogeneous catalysis are combined and well-defined materials with uniform active sites of equal activity towards the reactants can be made accessible for new catalytic applications.[14,15] Molecular pincer catalysts have been immobilized on different supports, mainly on silica and metal oxides[2,13,16–23] as well as metal-organic frameworks[24–28] or even microporous polymer networks,[29] but the resulting materials were mostly investigated for stoichiometric transformation,[30] coupled with metathesis[31] or transfer dehydrogenations,[2,32] whereas direct dehydrogenations remain underexplored.[13,22] Besides the high porosity and chemical robustness, the advantage of using a microporous polymer network (MPN) as support material is the tunable environment of the catalyst, as the polymer backbone can be versatilely functionalized.

Herein, the immobilization of an organometallic iridium pincer complex on a post-modified high-surface-area MPN is presented (Scheme 1), as well as its application in a catalytic continuous-flow dehydrogenation reaction. The novel MPN provides an inert environment with isolated anchor points for the immobilization of the metal-organic complex, ensuring the formation of a single-site catalyst.

We and others have recently shown the immobilization of iridium pincer complexes.[23,29] In these examples the complex has been conveniently anchored via the Ir center to OH-functional groups present on the surface of the support, yielding immobilized Ir(III) pincer complexes, which showed high activity in the hydrogenation of alkenes. However, such catalysts will not be active in the, industrially more important back reaction, i.e. the endothermic dehydrogenation of alkanes.

[a] M. König,[+] M. Traxler,[+] Dr. J. Schmidt, H. Küçükkeçeci, Prof. A. Thomas
Institut für Chemie
Technische Universität Berlin
Hardenbergstrasse 40
10623 Berlin (Germany)
E-mail: arne.thomas@tu-berlin.de
Homepage: https://www.funktionsmaterialien.tu-berlin.de
[b] M. A. Rudolph, Prof. R. Schomäcker
Institut für Chemie
Technische Universität Berlin
Straße des 17. Juni 124
10623 Berlin (Germany)
[+] These authors contributed equally.
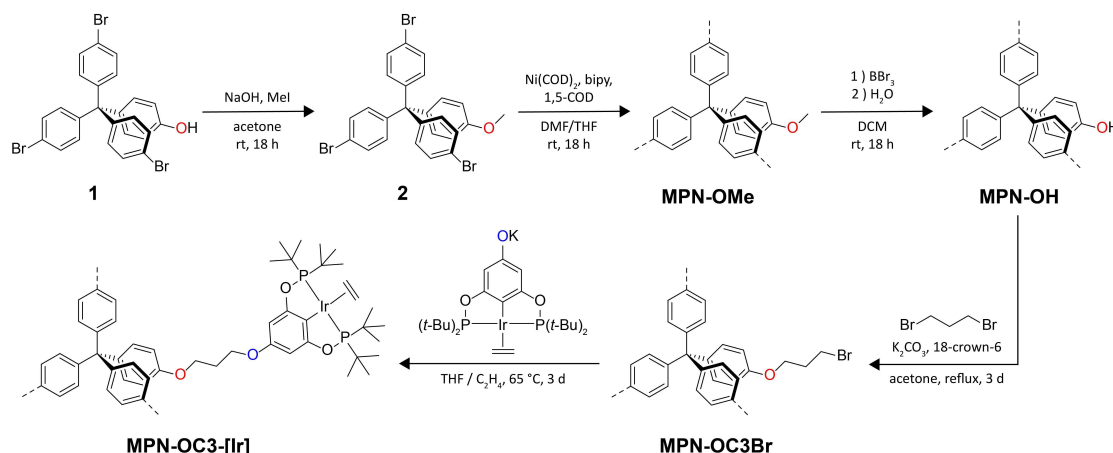
Scheme 1. Synthesis of methoxytetraphenylmethane polymer MPN-OMe, post-synthetic modification towards hydroxy functionalized MPN-OH and alkylated MPN-OC3Br and subsequent immobilization of iridium pincer complex {p-KO-C$_6$H$_2$-2,6-[OP(t-Bu)$_2$]$_2$}Ir(C$_2$H$_4$) yielding MPN-OC3-[Ir].

For the latter reaction, the central iridium atom of the pincer catalyst cannot be anchored directly to the support material, as for an effective dehydrogenation reaction an Ir(I) catalyst is required to ensure an Ir(I)-Ir(III) couple.[13] Therefore, the pincer complex has to be anchored to the support via the organic ligand.[2] In this study, a synthesis route for the immobilization of a potassium phenolate substituted pincer catalyst onto a propyl bromide-functionalized MPN is presented (Scheme 1). Notably, the catalyst synthesis includes three post-synthetic modification steps on the pre-formed MPN, but can be carried out with high efficiency.

Results and Discussion

In our previous work, we developed a synthetic route to provide a highly porous polymer network with isolated, reactive hydroxy functionalities as anchor points for further post-synthetic modifications.[29] To create such an OH-functionalized network, tris(4-bromophenyl)-methanol[33] was synthesized and converted into 4-hydroxyphenyl-tris(4-bromophenyl)methane **1**. To avoid possible interactions with the utilized metal species during polymerization, the hydroxy group was protected by methylation to yield 4-methoxyphenyl-tris(4-bromophenyl)-methane **2**. Subsequently, the protected monomer (**2**) was successfully converted to a methoxy functionalized microporous polymer network **MPN–OMe** with a SA_{BET} of 1014 m^{2}g^{-1} using nickel-mediated Yamamoto polymerization.[34] To recover the hydroxy group the methylated polymer **MPN–OMe** was quantitatively deprotected by successive treatment with BBr$_3$ and H$_2$O to yield a microporous polymer **MPN–OH** with a SA_{BET} of 911 m^{2}g^{-1} (Figure 1a).

As an anchoring point of an iridium pincer complex via its ligand, a small chain alkyl bromide needed to be introduced to the microporous polymer network. In order to find out a suitable chain length, which reacts efficiently with the phenolic OH groups of the polymer, but is sufficiently short not to block
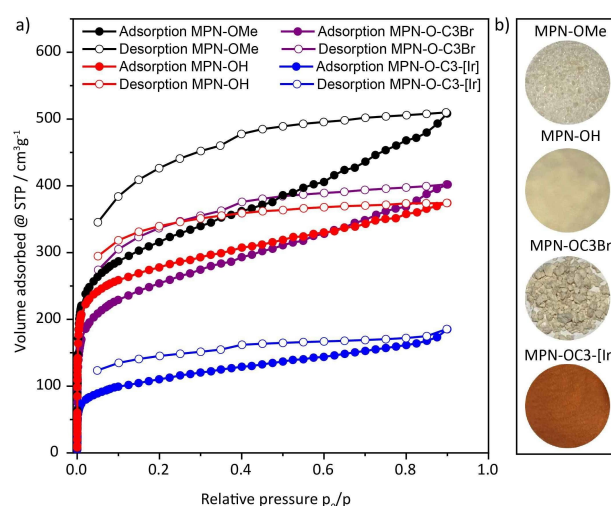

Figure 1. a) Ar sorption analysis at 87 K of **MPN–OMe** (black), **MPN–OH** (red), **MPN–OC3Br** (purple) and **MPN–O–[Ir]** (blue). b) Optical images of **MPN–OMe, MPN–OH, MPN–OC3Br** and **MPN–OC3–[Ir]**.

the pores of the polymer network, 1,2-dibromoethane, 1,3-dibromopropane and 1,4-dibromobutane were tested in the reaction with the model compound 4-tritylphenol using different reaction protocols. Low yields and slow conversion were obtained when introducing the bromoethyl chain. On the contrary, a reaction protocol using potassium carbonate and 18-crown-6 gave high conversion rates for the respective bromopropyl and bromobutyl ethers after reflux in acetone, respectively. Therefore, the same reaction protocol was applied for the post-synthetic modification of the **MPN–OH** polymer. For both chain lengths, a nearly quantitative conversion of the hydroxy groups of the microporous polymer was obtained, yielding in the formation of **MPN–OC3Br** and **MPN–OC4Br**. ^{13}C CP/MAS-NMR spectroscopy confirmed the successful attachment of the bromoalkyl chains since new signals in the region between 27 and 32 ppm could be identified as the signals for the aliphatic carbons of the alkyl chains. Furthermore, a low-

ChemCatChem

Research Article
doi.org/10.1002/cctc.202200811

**Chemistry
Europe**
European Chemical
Societies Publishing

field shift of the C_{Ar}—O signal from 154 to 157 ppm is observed, which also proves the assumed conversion of hydroxy to ether groups (Figure 2a [**MPN**—**OC3Br**]; Figure S1 [**MPN**—**OC4Br**]). Additionally, the complete conversion of the OH group to the respective bromoalkyl ether was confirmed by FT-IR, where the characteristic band around 3500 cm^{-1}, corresponding to O—H stretching, disappeared (Figure S4). Both functionalized polymer networks maintained their microporous characteristics and exhibit a SA_{BET} determined from Ar sorption experiments of 796 m^2 g^{-1} for **MPN**—**OC3Br** (Figure 1a) and 781 m^2 g^{-1} for **MPN**—**OC4Br** (Figure S5). Such a decrease of the SA_{BET} is expected due to the increase in molecular weight of the repeating units, plus the partial pore blockage of dangling bromoalkyl chains. As both chain lengths yield comparable results, further post-modification steps were carried out on **MPN**—**OC3Br**.

For anchoring the pincer complex onto the support, a potassium phenolate substituted pincer catalyst was prepared in the next step. The tridentate iridium pincer complex {p-KO-C_6H_2-2,6-[OP(t-Bu)$_2$]$_2$}Ir(C_2H_4) was synthesized according to the literature (Scheme S2).[2]

Then, {p-KO-C_6H_2-2,6-[OP(t-Bu)$_2$]$_2$}Ir(C_2H_4) was added to a suspension of **MPN**—**OC3Br** in THF under inert conditions. While stirring for 3 days under C_2H_4 atmosphere the polymer swelled and its color turned from beige to red (Figure 1b). Filtration,

Figure 2. a) Demethylation, post-synthetic modification and immobilization of Ir pincer complex monitored by ^{13}C CP/MAS-NMR spectroscopy: **MPN**—**OMe** (black), **MPN**—**OH** (red), **MPN**—**OC3Br** (purple) and immobilized Ir pincer complex **MPN**—**OC3**—**[Ir]** (blue). b) ^{31}P MAS-NMR spectroscopy of pincer complex {p-KO-C_6H_2-2,6-[OP(t-Bu)$_2$]$_2$}Ir(C_2H_4) (top), molecular model compound (middle) and immobilized iridium pincer complex **MPN**—**OC3**—**[Ir]** (bottom). Asterisks denote spinning sidebands.

extensive washing and drying in vacuum yielded the immobilized iridium pincer complex **MPN**—**OC3**—**[Ir]** (Scheme 1). To explore the binding situation of the immobilized pincer complex on the MPN support, a model compound featuring the repeating unit of the porous polymer was synthesized and analyzed by ^{1}H and ^{13}C liquid state NMR as well (supporting information).

The successful immobilization of the iridium pincer complex was again confirmed by solid-state NMR spectroscopy (Figure 2a). In the ^{13}C CP/MAS-NMR spectrum additional peaks in the aromatic region at 168, 160, and 92 ppm are observed attributed to the aromatic backbone of the pincer ligand. In addition, the signal at 28 ppm can be assigned to the methyl groups of the *tert*-butyl moiety and the signal at 41 ppm can be assigned to the quaternary *tert*-butyl carbon atom. The signal at 35 ppm can be equally assigned to the center aliphatic carbon of the C3-alkyl chain and the coordinated C_2H_4 molecules. When compared to the model compound, the signal at 67 ppm can be assigned to oxygen-connected aliphatic carbons of the alkyl chain. The peak broadening of the aromatic signal at 131 ppm is presumably due to an overlap with the spinning sideband of the signal of the *tert*-butyl methyl groups at 28 ppm. Small amounts of residual THF can be assumed due to the relatively sharp signals at 25 and 67 ppm. The ^{31}P MAS-NMR spectrum further confirms that the pincer ligand stays intact after immobilization as its chemical shift of 179 ppm closely resembles the value of the molecular complex and the designed model compound (Figure 2b).

After immobilization of the iridium pincer catalyst, the porosity of **MPN**—**OC3**—**[Ir]** was evaluated by low-pressure argon sorption studies. The material exhibits still a microporous character and the SA_{BET} was determined to be 360 m^2 g^{-1}. A decrease of SA_{BET} was expected due to the addition of the iridium complex with its bulky functional groups, which increases the weight of the repeating units and occupies the free volume of the MPN. Also, the apparent pore size calculated from the adsorption isotherm decreased after catalyst immobilization from 0.65 for **MPN**—**OC3Br** to 0.58 nm for **MPN**—**OC3**—**[Ir]** (Figure S7).

X-ray photoelectron spectroscopy (XPS) analysis of the iridium pincer complex, {p-KO-C_6H_2-2,6-[OP(t-Bu)$_2$]$_2$}Ir(C_2H_4), and the immobilized iridium pincer complex, **MPN**—**OC3**—**[Ir]**, were conducted to provide further evidence for the anchoring of the catalyst onto the polymer. The molecular metal-organic complex shows two peaks in the O 1s core-level spectrum at 532.0 and 533.3 eV, which both are in the binding energy range of organic oxygen compounds (Figure 3a). Additionally, the characteristic doublet at 131.6 eV in the P 2p spectrum can be assigned to the P—O species. In the Ir 4f spectrum, two different species with characteristic doublets at 60.6 and 63.7 eV, as well as 61.9 and 65.0 eV, can be detected. The set of lower binding energy can be attributed to the unchanged Ir(I) complex, while the peaks for higher binding energy are in the range of Ir(III) species.[29] This oxidation is most likely resulting from the transfer of the catalyst sample to the XPS measurement chamber and is limited to the outer surface of the material. In
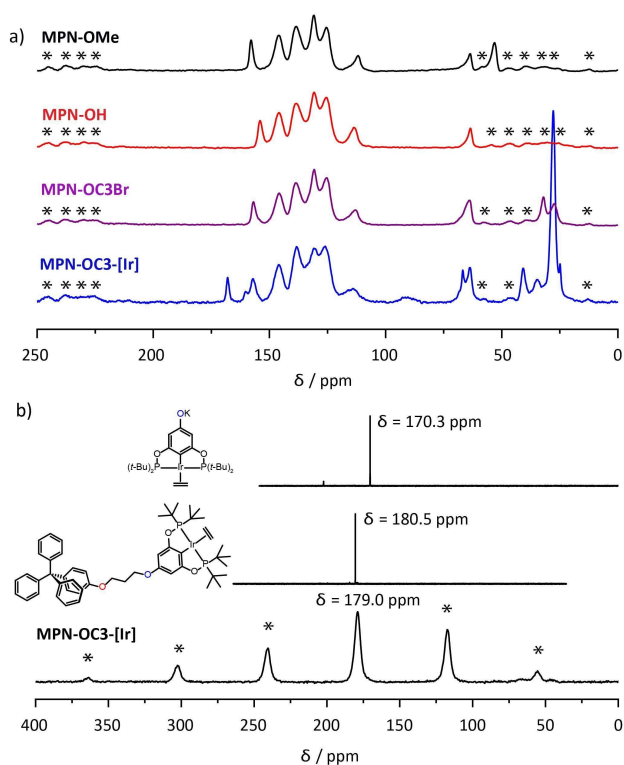
ChemCatChem

Research Article
doi.org/10.1002/cctc.202200811

Chemistry Europe
European Chemical
Societies Publishing

Figure 3. a) O 1s, P 2p and Ir 4f XPS spectra of {p-KO-C$_6$H$_2$-2,6-[OP(t-Bu)$_2$]$_2$} Ir(C$_2$H$_4$). b) O 1s, P 2p and Ir 4f XPS spectra of immobilized iridium pincer complex **MPN−OC3−[Ir]**. (Light grey – measured spectra; red line – fitted spectra; green and blue lines – fitted signals. c) Scanning electron microscopy and energy dispersive X-ray spectroscopic elemental mapping of **MPN−OC3−[Ir]**. Yellow belongs to iridium, blue belongs to phosphorus.

addition, the elemental ratio between iridium and phosphorus was determined as 2:1.

After the anchoring of the catalyst onto the surface of the microporous polymer network, the O 1s signals slightly shifted to 531.5 and 532.8 eV (Figure 3b). With the absence of a metal-oxygen species at lower binding energies it can be concluded, that the pincer complex is bound via the organic phenyl group rather than the iridium metal center. The P 2p spectrum and Ir 4f spectrum stay nearly identical to that of the molecular pincer catalyst. The extra peak at around 70 eV in the Ir 4f spectrum can be assigned to the Br 3d signal originating from KBr which is the side product of the substitution reaction of the anchoring. Finally, the elemental ratio for iridium and phosphorus in the porous polymer catalyst **MPN−OC3−[Ir]** stays 2:1, which confirms again the successful anchoring of the intact iridium pincer complex onto the porous polymer. In addition, the immobilization of the iridium pincer catalyst on the bromoalkyl modified model compound resulted in identical binding energies in the O 1s, P 2p and Ir 4f spectra **MPN−OC3−[Ir]** (Figure S11).

The iridium content was determined by inductively coupled plasma optical emission spectroscopy (ICP-OES) with a value of 7.9 wt%, indicating a functionalization degree of 41%. A spherical morphology of the MPN is seen by scanning electron microscopy (SEM). Elemental mapping shows the homogeneous distribution of iridium and phosphorus within **MPN−OC3−[Ir]** (Figure 3c). Following the results from solid-state NMR, XPS and SEM, it can be concluded, that the molecular iridium pincer complex has been successfully immobilized onto the microporous polymer support.

The immobilized iridium pincer complex was tested in the catalytic dehydrogenation of cyclohexane to benzene. Gaseous cyclohexane was used in a continuously operated experimental setup to enable simultaneous convenient temporal resolution with adequate experiment duration. To increase the bed height and to avoid potential hot spots, the porous polymer was mixed with SiC as inert material in a 1:9 mass ratio.

Two measurements with different temperature programs were conducted. The initial temperature ramp experiment was designed to find a suitable reaction temperature for the following isothermal stability test. In the first experiment, the catalyst was initially heated to 200 °C with a temperature ramp of 20 K min^{-1}. Subsequently, the activity of the catalyst was determined by holding at this temperature for 15 min. Then, with 4 K min^{-1} heating ramps followed by holding the temperature for 15 min, the temperature was increased in steps of 20 °C within the stability window of **MPN−OC3−[Ir]** to 340 °C (Figure 4a). The second measurement, using fresh catalyst material, consisted of heating with 5 K/min to 300 °C and holding for more than seven days (Figure 4b). An induction period is observed within the first 30 hours in which the activity of the catalysts is continuously rising. This might be due to an expansion of the highly cross-linked network during time, increasing the accessibility of active sites.

During both measurements, leakage (i.e. N$_2$, H$_2$O, O$_2$), combustion (CO$_x$), and partial dehydrogenation (cyclohexene) were not detected in a significant amount in comparison to the reference baselines. Consequently, total benzene selectivity is perceived. The feed consisting of argon, hydrogen, and cyclohexane was subject to minor fluctuations, but without impact on the formation of benzene. The co-feeding of hydrogen ensures a sufficient H$_2$ partial pressure for activating the catalyst to a dihydride complex in a plausible associative
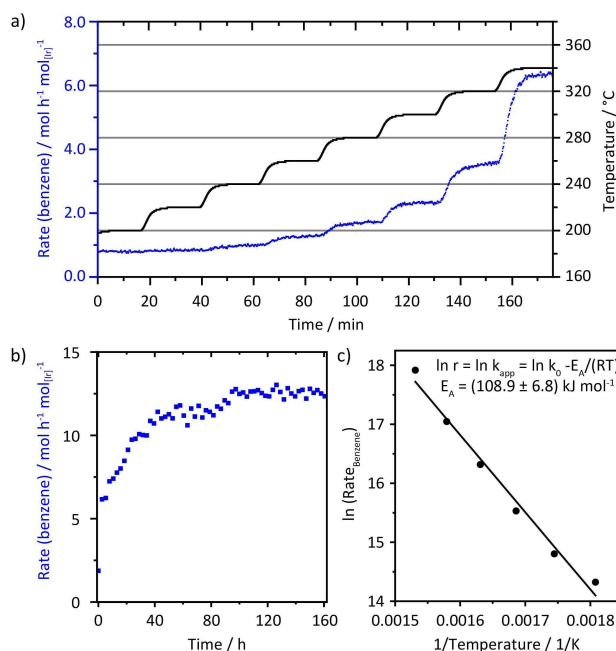

Figure 4. a) Catalytic dehydrogenation of cyclohexane. Temperature ramp measurement: Benzene formation rate depending on the catalyst bed temperature, heating with 4 K/min and holding for 15 min between 200 °C and 340 °C in steps of 20 °C. b) Isothermal stability measurement: Benzene formation rate at 300 °C for 168 h (figure neglects heating with 5 K/min to 300 °C). c) The rates of benzene formation during the steady regimes of each temperature step between 280 and 380 °C (except 380 °C in cycle 1) were averaged for each temperature. The temperature-rate pairs were used in an Arrhenius plot to determine the apparent activation energy of the dehydrogenation of cyclohexane to benzene of (108.9 ± 6.8) kJ mol^{-1}.

ChemCatChem

Research Article
doi.org/10.1002/cctc.202200811

Chemistry Europe
European Chemical
Societies Publishing

reaction mechanism, when performing temperature screening experiments starting with zero conversion.[35] Additionally, the hydrogen feed could also prevent possible C—H bond activation of the support by the iridium pincer complex. Furthermore, no benzene or other organic products could be detected in a reference reaction without the feed of cyclohexane, excluding that products are detected due to a decomposition of the polymer network or ligand.

The temperature ramping dehydrogenation of the **MPN—OC3—[Ir]** catalyst showed an increased formation of benzene, which is elevating with increasing temperature (Figure 4a). At 200 °C the yield of benzene in the dehydrogenation reaction was low. With increasing temperature the conversion of cyclohexane raised stepwise to a steady-state with a turnover frequency (TOF) of 6.3 mol h^{-1} mol$_{[Ir]}^{-1}$ at 340 °C. It is noteworthy that these temperatures are not accessible with unsupported molecular dehydrogenation catalysts, since the highest temperatures for those is considered 200–240 °C due to thermal instability.[36] Ramping the catalyst to temperatures beyond the stability window of the microporous dehydrogenation catalyst up to 400 °C led to a further increase in activity, with the highest benzene formation rates peaking as high as 99.5 mol h^{-1} mol$_{[Ir]}^{-1}$ at a cyclohexane conversion of more than 50 %. However, the initial rates at those temperatures are declining already within the 15 min holding phase (Figure S12). These results are in full agreement with findings from Sheludko et al. that the thermal decomposition product of the supported catalyst is retaining activity, even though at lower conversion rates.[13] Notably, the catalytic activity of the iridium pincer species is not affected by a co-feed of water (Figure S12, last cycle). This can be explained by the highly hydrophobic environment, which is provided by the microporous polymer network. This renders a further advantage of MPNs compared to other conventional, hydrophilic supports such as silica. The analysis of the temperature dependence of the reaction rates results in an apparent activation energy of (108.9 ± 6.8) kJ mol^{-1} (Figure 4c and supporting information), which is in accordance to simulations on Pt(111) surfaces.[37–39] The additionally performed Eyring plot confirms the activation enthalpy to be slightly higher than 100 kJ mol^{-1} and revealed a positive activation entropy of (55.0 ± 2.4) kJ mol^{-1} K^{-1} (Figure S14).

The following isothermal long time catalyst test showed – after an induction period of 24 h – a stable dehydrogenation of cyclohexane to benzene at a rate of 11.4 mol h^{-1} mol$_{[Ir]}^{-1}$ (Figure 4b), which relates to a conversion of 4.4 % of the theoretical maximum conversion based on thermodynamic simulations (Figure S15). This activity is comparable to reported silica-supported metal nanoparticle catalysts for the dehydrogenation of cyclohexane.[40–42] Additionally, the catalyst showed long-term stability with a turnover number higher than 1600. It should be noted, that the catalyst activity was stable for more than 7 days and no decrease in reaction rate was detected. The catalyst was analyzed after the long-term experiment using SEM and EDX analysis. The elemental mapping revealed, that both iridium and phosphorus are still distributed throughout the catalyst material (Figure S16).

Conclusion

In summary, herein we present a multi-step post-synthetically modified MPN as catalyst for the continuous flow dehydrogenation of cyclohexane to benzene. An iridium pincer complex was immobilized on an alkylated microporous polymer network with a resulting Ir content of 7.9 wt%. The successful immobilization of the intact pincer catalyst could be confirmed by solid-state ^{13}C and ^{31}P NMR spectroscopy. X-ray photoelectron spectroscopy validated the presence of the expected oxygen, phosphorus, and iridium species. Homogeneous distribution of iridium and phosphorus was confirmed by scanning electron microscopy. After immobilization, the SA_{BET} decreased from 796 to 360 m^2 g^{-1} due to the increased specific weight but without loss of the microporous characteristics. The catalytic performance was demonstrated in the continuous flow dehydrogenation of cyclohexane, where the material showed high long-term stability at a TOF of 11.4 mol h^{-1} mol$_{[Ir]}^{-1}$, which - to our knowledge - was not yet reported for the catalytic dehydrogenation of cyclohexane using an anchored metal organic catalyst. We believe that this highly tunable class of materials ensures the formation of single-site catalytically active species inside a chemically robust, inert, and hydrophobic polymer, offering ample opportunity for the field of surface organometallic chemistry due to the ability of the formation of tuned environments for the catalyst.

Experimental Section

Materials and methods. All chemicals were of reagent grade and used as received, and all experiments were carried out under Ar atmosphere if stated in the procedure. ^{11}B MAS, ^{13}C{^{1}H} CP/MAS and ^{31}P MAS measurements were carried out using a Bruker range Avance 400 MHz solid state spectrometer operating at a spinning rate of 10 kHz. Physisorption measurements were conducted at 87 K and Argon as sorption agent at relative pressures up to p/p$_0$ = 0.9 using an Autosorb-iQ-MP from Quantachrome. X-ray photoelectron spectra were measured on a K-Alpha™+ X-ray Photoelectron Spectrometer System (Thermo Scientific). Scanning electron microscopy images were recorded via ZEISS Gemini SEM 500 using NanoVP mode operating at 15 kV. For the energy dispersive spectroscopy, Bruker Quantax XFlash 6|60 detector was used.

Catalyst preparation. Hydroxytetraphenylmethane polymer **MPN—OH** was synthesized in accordance with a reported procedure.[29]

MPN—OC3Br. Polymer **MPN—OH** (525 mg, 1.58 mmol), K$_2$CO$_3$ (294 mg, 2.13 mmol) and a few crumbs of 18-crown-6 were suspended in acetone (60 mL). 1,3-Dibromopropane (0.98 mL, 9.62 mmol) was added via syringe and the reaction stirred at reflux for 3 days. After cooling down to room temperature the mixture was filtered off and the off-white precipitate washed with abundant amounts of water, acetone, THF and methanol. The product was purified via Soxhlet extraction from methanol overnight and dried at 80 °C in vacuum for 6 h to yield **MPN—OC3Br** as off-white powder. Yield, 620 mg (1.37 mmol repeating units, 87 %). ^{13}C{^{1}H} CP/MAS-NMR (100 MHz): δ = 157, 146, 138, 131, 125, 113, 64, 32, 27 ppm.

The potassium phenolate substituted pincer catalyst {*p*-KO-C$_6$H$_2$-2,6-[OP(*t*-Bu)$_2$]$_2$}Ir(C$_2$H$_4$) was prepared according to the literature.[2]

ChemCatChem

Research Article
doi.org/10.1002/cctc.202200811

Chemistry Europe
European Chemical
Societies Publishing

MPN−OC3−[Ir]. Polymer **MPN−OC3Br** (225 mg, 0.50 mmol) was added to a Schlenk flask and evacuated overnight. Under Ar atmosphere pincer catalyst {p-KO-C$_6$H$_2$-2,6-[OP(t-Bu)$_2$]$_2$}Ir(C$_2$H$_4$) (400 mg, 0.60 mmol) and THF (80 mL) were added. The THF suspension was degassed by three freeze-pump-thaw cycles. The flask was refilled with ethylene gas at −78 °C. The reaction stirred at 65 °C for 3 days. After cooling down to room temperature the solvent was removed via filtration under Ar atmosphere and the orange solid was washed with THF (6×20 mL) to remove the excess of metal precursor. The volatiles were removed under high vacuum (10^{-3} mbar), and the orange solid was dried under high vacuum (10^{-3} mbar) overnight. Drying in vacuum overnight (14 h) yielded the product as a red powder. ^{13}C{^{1}H} CP/MAS-NMR (100 MHz): δ = 168, 160, 157, 146, 138, 131, 126, 114, 92, 67, 64, 41, 35, 28, 25 ppm. ^{31}P{H} CP/MAS-NMR (162 MHz): δ = 179 ppm.

The model compound Tritylphenolate Pincer Complex (**10**) was synthesized similar to **MPN−OC3−[Ir]** but using 4-(3-bromo-propyloxy)tetraphenylmethane (**9**) as a representative unit of the polymer **MPN−OC3Br** (see SI).

Procedure for the dehydrogenation of cyclohexane using MPN−OC3-[Ir]. The catalytic performance was examined in a tubular fixed bed reactor (tapered quartz tube with a 4 mm inner diameter) with Swagelok Ultra-Torr fittings and Quick-Connects ensuring gas tightness against atmospheric oxygen and moisture. The reactor was placed vertically in a programmable oven (HTM Reetz). The feed of Argon (29 mL/min, 99.999%, Air Liquide) and hydrogen (1 mL/min, 99.999%, Air Liquide) was controlled by mass flow controllers (MFCs, Bronkhorst EL-FLOW) which were calibrated by a flow meter (Analyt-MTC). Argon was bubbled into a doubled walled gas-washing bottle (length 24 cm, frit VitraPOR filter plate with porosity 3) filled with cyclohexane (99.5%, Roth) which was held at 15 °C by a thermostat (Lauda Eco RE620). Argon, hydrogen and cyclohexane were used without further purification. The calibration of the cyclohexane feed was conducted measuring the evaporated volume of cyclohexane depending on the time. The decrease in cyclohexane volume in the gas-washing bottle or the difference in residence time of the Argon bubbles within the gas-washing bottle is neglectable. To ensure a stationary feed composition, the MFCs were run one hour in advance of the actual measurement. The feed composition was analysed by a mass spectrometer (GAM 200, InProcess Instruments) with a time resolution of 0.95 measurements of all the 11 channels per second detecting minimal fluctuations. The gas species and their respective channels (mass per charge ratio, m/z) are listed in Table S1. Cyclohexane and cyclohexene were measured via two channels due to overlapping molecular fractions. To calibrate the signals, a reference measurement excluding MPN−OC3−[Ir] was conducted at room temperature receiving the signal intensities correlated to zero cyclohexane conversion. The catalyst material (15.5 mg of MPN−OC3−[Ir] diluted with SiC (1:9 mass related, VWR, 100–500 μm) was mixed and placed on quartz wool (Roth) which was stabilized on the taper under inert conditions. With a bed height of 0.5 cm and a tube diameter of 4 mm, the residence time was 0.5 s.

Conflict of Interest

The authors declare no conflict of interest.

Data Availability Statement

The data that support the findings of this study are available from the corresponding author upon reasonable request.

[1] K. Das, A. Kumar, *Adv. Organomet. Chem.* **2019**, *72*, 1–57.
[2] Z. Huang, M. Brookhart, A. S. Goldman, S. Kundu, A. Ray, S. L. Scott, B. C. Vicente, *Adv. Synth. Catal.* **2009**, *351*, 188–206.
[3] J. T. Singleton, *Tetrahedron* **2003**, *59*, 1837–1857.
[4] Y. Wang, Z. Huang, X. Leng, H. Zhu, G. Liu, Z. Huang, *J. Am. Chem. Soc.* **2018**, *140*, 4417–4429.
[5] M. E. van der Boom, D. Milstein, *Chem. Rev.* **2003**, *103*, 1759–1792.
[6] N. Selander, K. J. Szabó, *Chem. Rev.* **2011**, *111*, 2048–2076.
[7] J. Choi, A. H. R. MacArthur, M. Brookhart, A. S. Goldman, *Chem. Rev.* **2011**, *111*, 1761–1779.
[8] A. Kumar, T. M. Bhatti, A. S. Goldman, *Chem. Rev.* **2017**, *117*, 12357–12384.
[9] L. Maser, L. Vondung, R. Langer, *Polyhedron* **2018**, *143*, 28–42.
[10] M. A. W. Lawrence, K.-A. Green, P. N. Nelson, S. C. Lorraine, *Polyhedron* **2018**, *143*, 11–27.
[11] E. Peris, R. H. Crabtree, *Chem. Soc. Rev.* **2018**, *47*, 1959–1968.
[12] X. Zhou, S. Malakar, T. Dugan, K. Wang, A. Sattler, D. O. Marler, T. J. Emge, K. Krogh-Jespersen, A. S. Goldman, *ACS Catal.* **2021**, *11*, 14194–14209.
[13] B. Sheludko, M. T. Cunningham, A. S. Goldman, F. E. Celik, *ACS Catal.* **2018**, *8*, 7828–7841.
[14] C. Copéret, M. Chabanas, R. Petroff Saint-Arroman, J.-M. Basset, *Angew. Chem. Int. Ed.* **2003**, *42*, 156–181; *Angew. Chem.* **2003**, *115*, 164–191.
[15] M. D. Korzyński, C. Copéret, *Trends Chem.* **2021**, *3*, 850–862.
[16] C. del Pozo, A. Corma, M. Iglesias, F. Sánchez, *Organometallics* **2010**, *29*, 4491–4498.
[17] M. Rimoldi, A. Mezzetti, *Inorg. Chem.* **2014**, *53*, 11974–11984.
[18] E. K. Huang, W.-M. Cheung, K.-W. Chan, F. L.-Y. Lam, X. Hu, Q.-F. Zhang, I. D. Williams, W.-H. Leung, *Eur. J. Inorg. Chem.* **2013**, 2893–2899.
[19] J. Ternel, L. Delevoye, F. Agbossou-Niedercorn, T. Roisnel, R. M. Gauvin, C. M. Thomas, *Dalton Trans.* **2010**, *39*, 3802.
[20] M. Rimoldi, A. Mezzetti, *Helv. Chim. Acta* **2016**, *99*, 908–915.
[21] M. Rimoldi, D. Fodor, J. A. van Bokhoven, A. Mezzetti, *Catal. Sci. Technol.* **2015**, *5*, 4575–4586.
[22] B. Sheludko, C. F. Castro, A. S. Goldman, F. E. Celik, *ACS Catal.* **2020**, *10*, 12425–12436.
[23] M. Rimoldi, D. Fodor, J. A. van Bokhoven, A. Mezzetti, *Chem. Commun.* **2013**, *49*, 11314–11316.
[24] S. A. Burgess, A. Kassie, S. A. Baranowski, K. J. Fritzsching, K. Schmidt-Rohr, C. M. Brown, C. R. Wade, *J. Am. Chem. Soc.* **2016**, *138*, 1780–1783.
[25] M. Rimoldi, A. Nakamura, N. A. Vermeulen, J. J. Henkelis, A. K. Blackburn, J. T. Hupp, J. F. Stoddart, O. K. Farha, *Chem. Sci.* **2016**, *7*, 4980–4984.
[26] A. M. Rasero-Almansa, A. Corma, M. Iglesias, F. Sánchez, *ChemCatChem* **2013**, *5*, 3092–3100.
[27] Y. Zhang, J. Li, X. Yang, P. Zhang, J. Pang, B. Li, H.-C. Zhou, *Chem. Commun.* **2019**, *55*, 2023–2026.
[28] B. R. Reiner, N. T. Mucha, A. Rothstein, J. S. Temme, P. Duan, K. Schmidt-Rohr, B. M. Foxman, C. R. Wade, *Inorg. Chem.* **2018**, *57*, 2663–2672.
[29] M. König, M. Rigo, N. Chaoui, T. Tran Ngoc, J. D. Epping, J. Schmidt, P. Pachfule, M. Ye, M. Trunk, J. F. Teichert, M. Drieß, A. Thomas, *Angew.*

ChemCatChem

Research Article
doi.org/10.1002/cctc.202200811

Chemistry Europe
European Chemical
Societies Publishing

Chem. Int. Ed. **2020**, *59*, 19830–19834; *Angew. Chem.* **2020**, *132*, 20002–20006.

[30] Z. H. Syed, D. M. Kaphan, F. A. Perras, M. Pruski, M. S. Ferrandon, E. C. Wegener, G. Celik, J. Wen, C. Liu, F. Dogan, K. I. Goldberg, M. Delferro, *J. Am. Chem. Soc.* **2019**, *141*, 6325–6337.

[31] Z. Huang, E. Rolfe, E. C. Carson, M. Brookhart, A. S. Goldman, S. H. El-Khalafy, A. H. Roy MacArthur, *Adv. Synth. Catal.* **2010**, *352*, 125–135.

[32] B. Sheludko, C. F. Castro, C. A. Khalap, T. J. Emge, A. S. Goldman, F. E. Celik, *ChemCatChem* **2021**, *13*, 407–415.

[33] K. Nikitin, E. Lestini, M. Lazzari, S. Altobello, D. Fitzmaurice, *Langmuir* **2007**, *23*, 12147–12153.

[34] J. Schmidt, M. Werner, A. Thomas, *Macromolecules* **2009**, *42*, 4426–4429.

[35] K. Krogh-Jespersen, M. Czerw, N. Summa, K. B. Renkema, P. D. Achord, A. S. Goldman, *J. Am. Chem. Soc.* **2002**, *124*, 11404–11416.

[36] G. E. Dobereiner, R. H. Crabtree, *Chem. Rev.* **2010**, *110*, 681–703.

[37] B. E. Koel, D. A. Blank, E. A. Carter, *J. Mol. Catal. A* **1998**, *131*, 39–53.

[38] M. Saeys, M. F. Reyniers, M. Neurock, G. B. Marin, *J. Phys. Chem. B* **2005**, *109*, 2064–2073.

[39] M. K. Sabbe, G. Canduela-Rodriguez, M. F. Reyniers, G. B. Marin, *J. Catal.* **2015**, *330*, 406–422.

[40] Z. Xia, H. Lu, H. Liu, Z. Zhang, Y. Chen, *Catal. Commun.* **2017**, *90*, 39–42.

[41] Z. Xia, H. Liu, H. Lu, Z. Zhang, Y. Chen, *Catal. Lett.* **2017**, *147*, 1295–1302.

[42] Z. Xia, H. Liu, H. Lu, Z. Zhang, Y. Chen, *Appl. Surf. Sci.* **2017**, *422*, 905–912.